



1 **Quantifying climate feedbacks in the**
2 **middle atmosphere using WACCM**

3
4 Maartje Sanne Kuilman¹, Qiong Zhang², Ming Cai³, Qin Wen^{1,4}

- 5
6 1. Department of Meteorology and Bolin Centre for Climate Research,
7 Stockholm University, Stockholm, Sweden
8 2. Department of Physical Geography and Bolin Centre for Climate
9 Research, Stockholm University, Stockholm, Sweden
10 3. Department of Earth, Ocean and Atmospheric Science, Florida State
11 University, Tallahassee, Florida, USA
12 4. Laboratory for Climate and Ocean-Atmosphere Studies (LaCOAS),
13 Department of Atmospheric and Oceanic Sciences, School of Physics,
14 Peking University, Beijing, China

15
16 Corresponding author: Maartje Sanne Kuilman (maartje.kuilman@misu.su.se)

17
18 **Key points:**

- 19
20 • In a double CO₂ climate, the direct forcing of CO₂ would lead to a
21 cooling of approximately 9 K in the middle atmosphere.
22
23 • The ozone feedback mitigates this cooling by warming the middle
24 atmosphere by approximately 1.5 K.
25
26 • The dynamical feedback is another important feedback with large
27 effects locally, while the effects of the water vapour feedback and
28 especially the cloud and albedo feedbacks are small.
29
30
31
32
33
34
35
36
37
38
39
40
41
42
43
44
45
46
47
48



49 **Abstract**

50
51 The importance of feedback processes in the middle atmosphere for surface
52 and tropospheric climate is increasingly realized. To better understand
53 feedback processes in response to a doubling of CO₂ we use the climate
54 feedback response analysis method (CFRAM). We examine the middle
55 atmosphere response to CO₂ doubling with respect to the pre-industrial state
56 in the Whole Atmosphere Community Climate Model (WACCM). Globally, the
57 simulated temperature decrease between 200 and 0.01 hPa (~12-80 km) is
58 found to be -5.2 K in July and -5.5 K in January in WACCM. The CFRAM
59 calculations show that the direct forcing of CO₂ alone would lead to an even
60 stronger cooling of approximately 9 K in the middle atmosphere in both July
61 and January. This cooling is being mitigated by the combined effect of the
62 different feedback processes.

63 The contribution from the ozone feedback causes a warming of approximately
64 1.5 K, mitigating the cooling due to changes in CO₂. Changes in CO₂ also
65 lead to changes in the middle atmosphere dynamics. The changes in
66 dynamics play a large role locally, especially above 0.1 hPa. Other feedback
67 processes, which are known to be important in the tropospheric and surface
68 climate, such as the water vapor, albedo and cloud feedbacks are of minor
69 importance in the middle atmosphere, although some effects are seen in the
70 stratosphere, mainly through the responses to sea surface temperature and
71 sea ice changes. It should be noted that there is a relatively large error term
72 associated with the current method in the middle atmosphere, which can be
73 explained by the linearization in the method.

74
75 **1. Introduction**

76
77 The middle atmosphere is the region of the atmosphere that encompassed
78 the stratosphere, where the temperature increases with height, from 10-50 km
79 and the mesosphere, where the temperature decreases with height, from
80 about 50-90 km. A classic study by Manabe and Strickler (1964) shows that
81 in the troposphere, water vapour is the dominant greenhouse gas, followed by
82 CO₂. Ozone is responsible for the existence of the stratosphere and the
83 reversal of the temperature gradient in the stratosphere.

84
85 The middle atmosphere is generally controlled by radiative processes
86 although there are important exceptions. The temperature in the winter
87 stratosphere for example, is significantly greater than what is expected from
88 radiative equilibrium considerations alone. This results from adiabatic heating
89 associated with downwelling at higher latitudes as a part of the Brewer-
90 Dobson circulation (Brewer, 1949, Dobson, 1956).

91
92 Many chemical, physical and dynamical processes in the middle atmosphere
93 are still often overlooked in climate model simulations. This can be noticed
94 from the description of the experimental design in model intercomparison
95 projects as in e.g. *Kageyama et al. (2017)* and *Taylor et al. (2012)*. However,
96 recently, there have been a number of studies that show the importance of the
97 middle atmosphere for the surface and tropospheric climate. It has, for



98 example, been shown that cold winters in Siberia are linked to changes in the
99 stratospheric circulation (*Zhang et al.*, 2018).

100 Other studies show that the representation of ozone in climate models affects
101 climate change projections (*Dietmüller et al.*, 2014; *Noda et al.*, 2017; *Nowack*
102 *et al.*, 2015, 2018;). It has been found that the ozone representation can result
103 in up to a 20% difference in simulated global mean surface warming (*Nowack*
104 *et al.*, 2015), although the exact importance of changes in ozone seems to be
105 dependent on both the model and the scenario (*Nowack et al.*, 2015) and is
106 not found by all studies (*Marsh et al.*, 2016).

107 Neglecting the effect of ozone may lead to a significant underestimation of the
108 temperature during past climate if we compare with available paleoclimate
109 reconstructions (*Ljungqvist et al.*, 2019), and may also alter the future climate
110 projections in different CO₂ scenarios. As the effect is found to be rather large
111 in some studies, and absent in other, there is a need for a better
112 understanding of the behaviour of the middle atmosphere in response to
113 changing CO₂ conditions, as the ozone concentration is influenced by this.
114

115 Ozone is an example of a climate feedback, a process that changes in
116 response to a change in CO₂-concentration and in turn dampens or amplifies
117 the climate response to the CO₂ perturbation. These climate feedbacks are a
118 challenging subject of study, as observed climate variations might not be in
119 equilibrium, multiple processes are operating at the same time and moreover
120 the geographical structures and timescales of different forcings differ.
121 However, feedbacks form a crucial part of understanding the response of the
122 atmosphere to changes in the CO₂-concentration.

123 Various methods have been developed to study these feedbacks, such as the
124 partial radiative perturbation (PRP) method, the online feedback suppression
125 approach and the radiative kernel method (*Bony et al.*, 2006 and the
126 references therein). These methods study the origin of the global climate
127 sensitivity (*Soden and Held*, 2006; *Caldwell et al.*, 2016; *Rieger et al.*, 2017).
128 The focus of these methods is on changes in the global mean surface
129 temperature, global mean surface heat and global mean sensible heat fluxes
130 (*Ramaswamy et al.*, 2019).

131 These methods are powerful for this purpose, however, they are not suitable
132 to explain temperature changes on spatially limited domains. They neglect
133 non-radiative interactions between feedback processes and they only account
134 for feedbacks that directly affect the radiation at the top of the atmosphere
135 (TOA).

136 Recently, a new climate feedback analysis method has been developed,
137 which is an offline diagnostic tool: the climate feedback-response analysis
138 method (CFRAM). With this method, one can calculate the temperature
139 changes on a spatially limited domain: it is possible to isolate partial
140 temperature changes due to an external forcing and internal feedbacks in the
141 atmosphere. The partial temperature changes are linearly addable; their sum
142 is equal to the total temperature change (*Cai and Lu*, 2009, *Lu and Cai*,



143 2009).

144

145 CFRAM takes into account that the climate change is not only determined by
146 the energy exchange between the Earth's system and outer space, but is also
147 influenced by the energy flow within the Earth's system itself. The method is
148 based on the energy balance in an atmosphere-surface column. It solves the
149 linearized infrared radiation transfer model for the individual energy flux
150 perturbations.

151

152 As a practical diagnostic tool to analyse the role of various forcing and
153 feedback, CFRAM has been used widely in climate change research on
154 studying surface climate change (*Taylor et al.*, 2013; *Song and Zhang*, 2014;
155 *Hu et al.*, 2017; *Zheng et al.*, 2019).

156

157 This method has been applied to the middle atmosphere climate sensitivity
158 study as well (*Zhu et al.*, 2016). In that study, the CFRAM method has been
159 adapted and applied to both model output, as well as observations. They
160 study the atmosphere responses during solar maximum and minimum and
161 find that the variation in solar flux forms the largest radiative component. They
162 show that increasing CO₂ cools the middle atmosphere, while the changes in
163 O₃-concentration lead to a cooling in some regions of the middle atmosphere
164 and to a warming in others.

165

166 In the present work, we apply CFRAM to climate sensitivity experiments
167 performed by the Whole Atmosphere Community Climate Model (WACCM),
168 which is a high-top global climate system model, including the full middle
169 atmosphere chemistry. We investigate the effects of doubling the CO₂-
170 concentration and the accompanying sea surface temperature changes on the
171 temperature changes in the middle atmosphere as compared to the pre-
172 industrial state. We discuss the total responses and feedbacks, as well as
173 those that are induced by doubling CO₂ and changes in the sea surface
174 temperature and sea ice distribution separately.

175

176 **2. The model and methods**

177

178 **2.1 Model description**

179 The Whole Atmosphere Community Model (WACCM) is a chemistry-climate
180 model, which spans the range of altitudes from the Earth's surface to about
181 140 km (*Marsh et al.*, 2013). The model consists of 66 vertical levels with
182 irregular resolution, ~1.1 km in the troposphere above the boundary layer,
183 1.1–1.4 km in the lower stratosphere, 1.75 km at the stratosphere and 3.5 km
184 above 65 km. The horizontal resolution is 1.9° latitude by 2.5° longitude.

185 WACCM is a superset of the Community Atmospheric Model version 4
186 (CAM4) developed at the National Center for Atmospheric Research (NCAR).
187 Therefore, WACCM includes all the physical parameterizations of CAM4
188 (*Neale et al.*, 2013), and a well-resolved high-top middle atmosphere. The
189 orographic gravity wave (GW) parameterization is based on *McFarlane*
190 (1987). WACCM also includes parameterized non-orographic GWs, which are



191 generated by frontal systems and convection (*Richter et al.*, 2010). The
192 parameterization of non-orographic GW propagation is based on the
193 formulation by *Lindzen* (1981).

194 The chemistry in WACCM is based on version 3 of the Model for Ozone and
195 Related Chemical Tracers (MOZART). This model represents chemical and
196 physical processes from the troposphere until the lower thermosphere.
197 (*Kinnison et al.*, 2007). In addition, WACCM simulates chemical heating,
198 molecular diffusion and ionization and gravity wave drag.

199 2.2 Experimental set-up

200 In this study, we first perform a simulation under pre-industrial conditions and
201 take this experiment as a control run, forced with pre-industrial ocean surface
202 conditions such as sea surface temperature and sea ice (referred to SSTs
203 from now on), see table 1. The pre-industrial CO₂-concentration is set as 280
204 ppm, the SSTs are from the CMIP5 pre-industrial control simulation by the
205 fully coupled earth system model CESM (*Hurrell et al.*, 2013). The atmosphere
206 component of CESM is the same as WACCM, but does not include
207 stratospheric chemistry.

208 We also run a perturbation experiment by doubling the CO₂ concentration to
209 560 ppm from pre-industrial level. In WACCM, the CO₂-concentration does
210 not double everywhere in the atmosphere. Only the surface level CO₂ mixing
211 ratio is doubled, and elsewhere in the atmosphere is calculated according to
212 WACCM's chemical model. For the double CO₂ simulation, we run two
213 experiments by using two SSTs forcing, one is keeping the pre-industrial
214 SSTs unchanged, and another one from a double CO₂ equilibrium simulation
215 by CESM. To investigate the effect of SSTs, we further run a simulation for
216 only using the SST forcing from the coupled CESM for double CO₂ condition,
217 but keep the CO₂-concentration as 280 ppm. All the simulations are run for 50
218 years, of which the last 40 years are used for analysis.

219 Table 1. Set-up of the model experiments.

Experiment	CO ₂	SSTs from CESM equilibrium run
Pre-industrial	280 ppm	PI control
CO ₂ and SSTs high	560 ppm	Double CO ₂ run
CO ₂ high	560 ppm	PI control
SSTs high	280 ppm	Double CO ₂ run

220 2.3 Climate feedback-response analysis method (CFRAM)

221 In this study, we aim to understand and quantify the different climate
222 feedbacks that may play a role in the middle atmosphere in a high CO₂
223 climate. For this purpose, we apply a climate feedback-response analysis
224 method (CFRAM).

225
226 As briefly discussed in the introduction, traditional methods to study climate
227 feedbacks are based on the energy balance at the top of the atmosphere



228 (TOA). This means that the only climate feedbacks that are taken into account
229 are those that effect the radiative balance at the TOA. However, there are
230 other thermodynamic and dynamical processes that do not directly affect the
231 TOA energy balance, while they do yield a temperature response in the
232 atmosphere.

233
234 Contrary to TOA-based methods, CFRAM considers all the radiative and non-
235 radiative feedbacks that result from the climate system due to response to an
236 external forcing. This means that CFRAM starts from a slightly different
237 definition of a feedback process. Note also that as the changes in temperature
238 are calculated simultaneously, the vertical mean temperature or lapse rate
239 feedback per definition do not exist in CFRAM.

240
241 Another advantage of CFRAM is that it allows for measuring the magnitude of
242 a certain feedback in units of temperature. We can actually calculate how
243 much of the temperature change is due to which process. The '*climate*
244 *response*' in the name of this method refers to the changes in temperature in
245 response to the climate forcings and climate feedbacks.

246
247 The mathematical formulation of CFRAM is based on the conservation of total
248 energy. At a given location in the atmosphere, the energy balance in an
249 atmosphere-surface column can be written as:

250
251
$$\vec{R} = \vec{S} + \vec{Q}^{conv} + \vec{Q}^{turb} - \vec{D}^v - \vec{D}^h + \vec{W}^{fric} \quad (1)$$

252
253 \vec{R} represents the vertical profile of the net long-wave radiation emitted by the
254 different layers in the atmosphere and surface. \vec{S} is the vertical profile of the
255 solar radiation, which is absorbed by these layers. \vec{Q}^{turb} is the convergence of
256 total energy in each layer due to turbulent motions, \vec{Q}^{conv} is convergence of
257 total energy into the layers due to convective motion. \vec{D}^v is the large-scale
258 vertical transport of energy from different layers to others. \vec{D}^h is the large-
259 scale horizontal transport within the layers and \vec{W}^{fric} is the work done by
260 atmospheric friction.

261
262 Due to an external forcing (in this study, the change in CO₂-concentration
263 and/or change in SSTs), the difference in the energy flux terms then
264 becomes:

265
266
$$\Delta\vec{R} = \Delta\vec{F}^{ext} + \Delta\vec{S} + \Delta\vec{Q}^{conv} + \Delta\vec{Q}^{turb} - \Delta\vec{D}^v - \Delta\vec{D}^h + \Delta\vec{W}^{fric} \quad (2)$$

267
268 In which the delta (Δ) stands for the difference between the perturbation run
269 and the control run.

270
271 CFRAM takes advantage of the fact that the infrared radiation is directly
272 related to the temperatures in the entire column. The temperature changes in
273 the equilibrium response to perturbations in the energy flux terms can be
274 calculated. This is done by requiring that the temperature-induced changes in
275 infrared radiation to balance the non-temperature induced energy flux



276 perturbations.

277

278 Equation (2) can also be written as:

279

$$280 \quad \Delta(\vec{S} - \vec{R})_{total} + \Delta dyn = 0 \quad (3)$$

281

282 The term $\Delta(\vec{S} - \vec{R})$ we can calculate as the longwave heating rate and the
283 solar heating rate are output variables of the model simulations. We then
284 calculate the difference in these heating rates for the perturbation simulation
285 and the control simulation.

286

287 We use the term $\Delta(\vec{S} - \vec{R})_{total}$ to calculate the dynamics term Δdyn .

288

$$289 \quad \Delta dyn = -\Delta(\vec{S} - \vec{R})_{total} \quad (4)$$

290

291 WACCM provides us with a heating rate in Ks^{-1} . For the CFRAM calculations,
292 we need the energy flux in Wm^{-2} . We can calculate the energy flux by
293 multiplying with the mass of different layers in the atmosphere and the specific
294 heat capacity.

295

$$296 \quad \Delta(\vec{S} - \vec{R}) = \Delta(\vec{S} - \vec{R})_{(WACCM)} * mass_k * c_p \quad (5)$$

297

298 with $mass_k = \frac{p_{k+1} - p_k}{g}$ with p in Pa and $c_p = 1004 \text{ J kg}^{-1} \text{ K}^{-1}$ the specific heat
299 capacity at constant pressure.

300

301 WACCM includes a non-local thermal equilibrium (non-LTE) radiation scheme
302 above 50 km. It consists of a long-wave radiation (LW) part and a short-wave
303 radiation (SW) part which includes the extreme ultraviolet (EUV) heating rate,
304 chemical potential heating rate, CO_2 near-infrared (NIR) heating rate, total
305 auroral heating rate and non-EUV photolysis heating rate.

306

307 Therefore, we split the term $\Delta(\vec{S} - \vec{R})_{total}$ in an LTE and a non-LTE term:

308

$$309 \quad \Delta(\vec{S} - \vec{R})_{total} = \Delta(\vec{S} - \vec{R})_{LTE} + \Delta(\vec{S} - \vec{R})_{non-LTE} \quad (6)$$

310

311 WACCM provides us with the total longwave heating rate as well as the total
312 solar heating rate and the non-LTE longwave and shortwave heating rates for
313 the different runs. This means that we can calculate the term $\Delta(\vec{S} - \vec{R})_{non-LTE}$
314 as well, where we again need to convert our result from Ks^{-1} to Wm^{-2} :

315

$$316 \quad \Delta(\vec{S} - \vec{R})_{non-LTE} = \Delta(\vec{S} - \vec{R})_{non-LTE(WACCM)} * mass_k * c_p \quad (7)$$

317

318 This term can be inserted in equation (3):

319

$$320 \quad \Delta(\vec{S} - \vec{R})_{LTE} + \Delta(\vec{S} - \vec{R})_{non-LTE} + \Delta dyn = 0 \quad (8)$$

321



322 The central step in CFRAM is to decompose the radiative flux vector, using a
323 a linear approximation.

324 We start by decomposing the LTE infrared radiative flux vector $\Delta\vec{R}$

325

$$326 \quad \Delta\vec{R}_{LTE} = \frac{\partial\vec{R}}{\partial T}\Delta T + \Delta\vec{R}_{CO_2} + \Delta\vec{R}_{O_3} + \Delta\vec{R}_{H_2O} + \Delta\vec{R}_{albedo} + \Delta\vec{R}_{cloud} \quad (9)$$

327

328 where $\Delta\vec{R}_{CO_2}$, $\Delta\vec{R}_{O_3}$, $\Delta\vec{R}_{H_2O}$, $\Delta\vec{R}_{albedo}$, $\Delta\vec{R}_{cloud}$ are the changes in infrared
329 radiative fluxes due to the changes in CO₂, ozone, water vapour, albedo and
330 clouds, respectively.

331

332 For equation (9), we assumed that radiative perturbations can be linearized by
333 neglecting the higher order terms of each thermodynamic feedback and the
334 interactions between these feedbacks. This is also commonly done in the
335 PRP method (Bony *et al.*, 2006).

336

337 The term $\frac{\partial\vec{R}}{\partial T}\Delta T$ represents the changes in the IR radiative fluxes related to the
338 temperature changes in the entire atmosphere-surface column. The matrix $\frac{\partial\vec{R}}{\partial T}$
339 is the Planck feedback matrix, in which the vertical profiles of the changes in
340 the divergence of radiative energy fluxes due to a temperature change are
341 represented.

342

343 We calculate this feedback matrix using the output variables of the
344 perturbation and the control run of WACCM and inserting these in the CFRAM
345 radiation code: atmospheric temperature, surface temperature, reference
346 height temperature, ozone, surface pressure, solar insolation, downwelling
347 solar flux at the surface, net solar flux at the surface, dew point temperature,
348 cloud fraction, cloud ice amount, cloud liquid amount, ozone and specific
349 humidity.

350

351 Similarly, the changes in the LTE shortwave radiation flux can be written as
352 the sum of the change in shortwave radiation flux due to the direct forcing of
353 CO₂ and the different feedbacks:

354

$$355 \quad \Delta\vec{S}_{LTE} = \Delta\vec{S}_{CO_2} + \Delta\vec{S}_{O_3} + \Delta\vec{S}_{H_2O} + \Delta\vec{S}_{albedo} + \Delta\vec{S}_{cloud} \quad (10)$$

356

357 Similarly, to equation (9), we perform a linearization.

358

359 Substituting (9) and (10) in equation (8) yields:

360

$$361 \quad \Delta(\vec{S} - \vec{R})_{CO_2} + \Delta(\vec{S} - \vec{R})_{O_3} + \Delta(\vec{S} - \vec{R})_{H_2O} + \Delta(\vec{S} - \vec{R})_{albedo} + \Delta(\vec{S} - \vec{R})_{cloud} - \frac{\partial\vec{R}}{\partial T}\Delta T$$
$$362 \quad + \Delta(\vec{S} - \vec{R})_{non-LTE} + \Delta dyn = 0 \quad (11)$$

363

364 This can be written as:

365

$$366 \quad \frac{\partial\vec{R}}{\partial T}\Delta T = +\Delta(\vec{S} - \vec{R})_{non-LTE} + \Delta dyn \quad (12)$$



367
368 Equation (12) can be solved for the individual temperature perturbations. We
369 calculate the temperature changes due to the direct effect of CO₂ as well as
370 the different feedback processes.
371

$$372 \Delta T_{CO_2} = \left(\frac{\partial \bar{R}}{\partial \bar{T}} \right)^{-1} \Delta(\vec{S} - \vec{R})_{CO_2} \quad (13)$$

373
374 This can be done in a similar way for the different feedback processes:
375

$$376 \Delta T_{O_3} = \left(\frac{\partial \bar{R}}{\partial \bar{T}} \right)^{-1} \Delta(\vec{S} - \vec{R})_{O_3} \quad (14)$$

$$377 \Delta T_{H_2O} = \left(\frac{\partial \bar{R}}{\partial \bar{T}} \right)^{-1} \Delta(\vec{S} - \vec{R})_{H_2O} \quad (15)$$

$$378 \Delta T_{albedo} = \left(\frac{\partial \bar{R}}{\partial \bar{T}} \right)^{-1} \Delta(\vec{S} - \vec{R})_{albedo} \quad (16)$$

$$380 \Delta T_{cloud} = \left(\frac{\partial \bar{R}}{\partial \bar{T}} \right)^{-1} \Delta(\vec{S} - \vec{R})_{cloud} \quad (17)$$

381
382 The factors $\Delta(\vec{S} - \vec{R})_{CO_2}$, $\Delta(\vec{S} - \vec{R})_{O_3}$, $\Delta(\vec{S} - \vec{R})_{H_2O}$, $\Delta(\vec{S} - \vec{R})_{albedo}$ and
383 $\Delta(\vec{S} - \vec{R})_{cloud}$ are calculated by inserting the output variables from WACCM in
384 the radiation code of CFRAM. Here, one takes the output variables from the
385 control run, apart from the variable that is related to the direct forcing or the
386 feedback.
387
388

389
390 This means that for the direct forcing of CO₂, one takes the CO₂ from the
391 perturbation run, while one takes the other variables from the control run. For
392 the ozone feedback, one takes the ozone from the perturbation run. For the
393 water vapour feedback, one takes the specific humidity, surface pressure,
394 surface temperature and dew point temperature. While for the albedo
395 feedback, one takes the downwelling solar flux at surface and net solar flux at
396 surface from the perturbation run and the other variables from the control run.
397 For the cloud feedback, one takes the cloud fraction, cloud ice and cloud
398 liquid amount from the perturbation run. For all these feedbacks, one takes
399 the other variables from the control run.
400

401 Similarly to equations (13)-(17), we also calculate the temperature change
402 due to non-LTE processes and the dynamical feedback. We already
403 calculated the terms $\Delta(\vec{S} - \vec{R})_{non-LTE}$ and Δdyn in (4) and (7).
404

$$405 \Delta T_{non-LTE} = \left(\frac{\partial \bar{R}}{\partial \bar{T}} \right)^{-1} \Delta(\vec{S} - \vec{R})_{non-LTE} \quad (18)$$

$$406 \Delta T_{dyn} = \left(\frac{\partial \bar{R}}{\partial \bar{T}} \right)^{-1} \Delta dyn \quad (19)$$

407
408 The calculated partial temperature changes can be added, their sum being
409



410 equal to the total temperature change. It is important to note that this does not
411 mean that the individual processes are physically independent of each other.

$$413 \Delta T_{CFRAM} = +\Delta T_{O_3} + \Delta T_{H_2O} + \Delta T_{albedo} + \Delta T_{cloud} + \Delta T_{non-LTE} + \Delta T_{dyn}$$

(20)

415 The linearization done for equations (9) and (10) introduces an error between
416 the temperature difference as calculated by CFRAM and as seen in the model
417 output. Another source of error is that the radiation code of the CFRAM
418 calculations is not exactly equal to the radiation code of WACCM.

$$420 \Delta T_{CFRAM} = \Delta T_{WACCM} - \Delta T_{error} \quad (21)$$

422 For more details on the CFRAM method, please refer to *Lu and Cai (2009)*.

424 Note that the method used in this study differs slightly from the Middle
425 Atmosphere Climate Feedback Response Analysis Method (MCFRAM) used
426 by *Zhu et al. (2016)*. The major difference is that in this study, we perform the
427 calculations using the units of energy fluxes (Wm^{-2}) instead of converting to
428 heating rates (Ks^{-1}). Another difference is that our method is not applicable
429 above 0.01 hPa (~ 80 km), while *Zhu et al. (2016)* added molecular thermal
430 conduction to the energy equation, to perform the calculations beyond the
431 mesopause.

433 3. Results

435 3.1 Temperature responses in a double CO₂ scenario

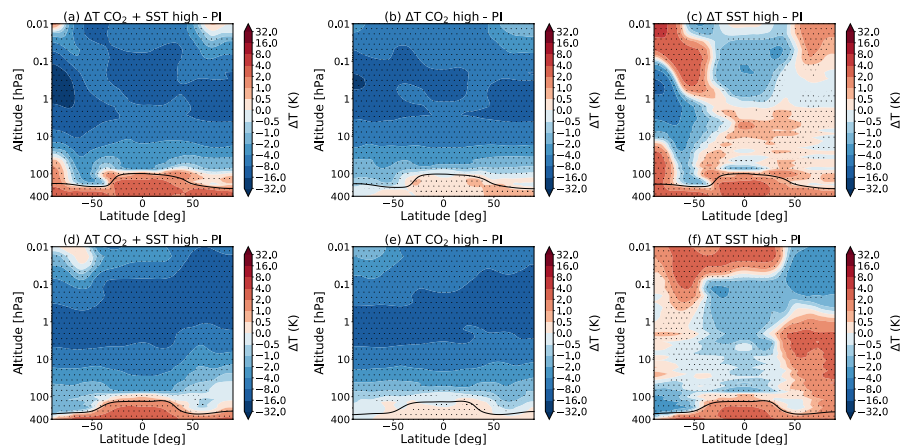
437 In section 2.2, it was discussed that four experiments were performed with
438 WACCM: a simulation with pre-industrial conditions, a simulation with
439 changed SSTs only, a simulation with only a changed CO₂-concentration and
440 a final simulation with both changed SSTs and CO₂-concentration.

442 Figure 1 shows the temperature changes for the different experiments with
443 respect to the pre-industrial state, as modelled by WACCM. As shown in
444 earlier studies, we observe that an increase in CO₂ causes a cooling in the
445 middle atmosphere with the exception of the cold summer upper mesosphere
446 region (*Akmaev, 2006*). We also observe that changing the SSTs alone, while
447 leaving the CO₂-concentration at the pre-industrial levels (Fig 1c and 1f) also
448 yields significant temperature changes over a large part of the middle
449 atmosphere, and contributes to the observed warming in the cold summer
450 mesopause region.

452 In line with *Fomichev et al. (2007)* and *Schmidt et al. (2006)*, we find that the
453 sum of the two separate temperature changes in the experiment with changed
454 CO₂ only and changed SSTs only is approximately equal to the changes
455 observed in the combined simulation. *Shepherd (2008)* has explained this
456 phenomenon as follows: climate change affects the middle atmosphere in two
457 ways: either radiatively through in situ changes associated with changes in
458 CO₂ or dynamically through changes in stratospheric wave forcing, which are
459 primarily a result of changing the SSTs (*Shepherd, 2008*). Even though the



460 radiative and dynamic processes are not independent, at first approximation,
461 these processes are seen to be additive (*Sigmond et al.*, 2004, *Schmidt et al.*,
462 2006, *Fomichev et al.*, 2007).
463



464
465 Figure 1: The total change in temperature in July (top) and January (bottom)
466 for (a,d) the simulation with high CO₂ and SSTs, (b,e) the simulation with high
467 CO₂, (c,f) the simulation with high SSTs, all as compared the pre-industrial
468 control simulation. The dotted regions indicate the regions where the data
469 reaches a confidence level of 95%. The black line indicates the tropopause
470 height for the runs with changed CO₂-concentration and SSTs (a,d), with
471 changed CO₂-concentration (b,e) and with changed SSTs (c,f).
472

473 The CFRAM makes it possible to separate and estimate the temperature
474 responses due to an external forcing and various climate feedbacks, such as
475 ozone, water vapour, cloud, albedo and dynamical feedbacks. Note that for
476 the ozone, water vapour, cloud and albedo feedback, we can only calculate
477 the radiative part of the feedback.
478

479 Because we are using an atmosphere-only model, in our experiment, the
480 external forcing is either the change in CO₂-concentration or the change in
481 SSTs or both. In an atmosphere-ocean model (such as CESM) and, of
482 course, in reality the changes in sea surface temperature and sea ice
483 distributions are responses to the changed CO₂-concentration.
484

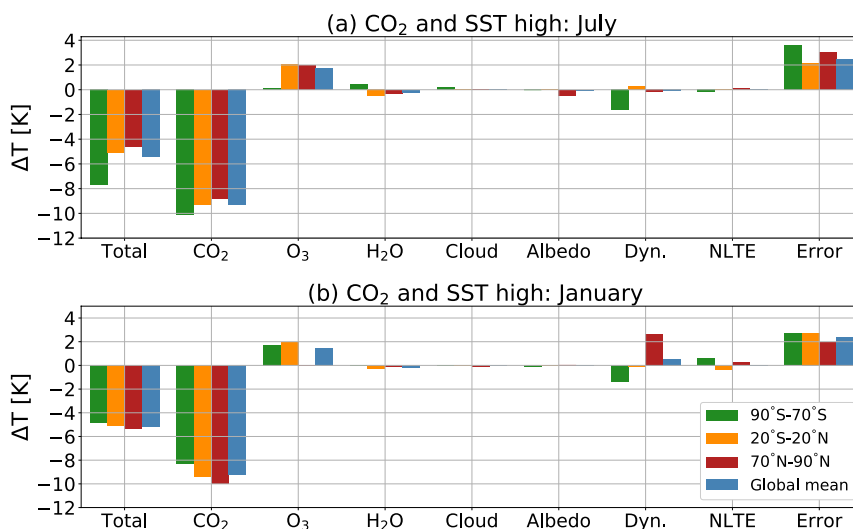
485
486 Figure 2 shows the average change in global mean temperature for the
487 middle atmosphere between 200 and 0.01 hPa (12-80 km) for the experiment
488 with the changed CO₂-concentration and changed SSTs. The 'total'-column
489 shows the temperature changes in WACCM. It is found that the average
490 change in global mean temperature for the middle atmosphere between 200
491 and 0.01 hPa for this experiment is approximately -5.5 K in July and -5.2 K in
492 January in WACCM.
493

494 Figure 2 also shows the radiative feedbacks due to ozone, water vapour,
495 clouds, albedo and the dynamical feedback, as well as the small contribution



496 due to the Non-LTE processes, as calculated by CFRAM. The column 'error'
497 shows the difference between temperature change in WACCM and the sum of
498 the calculated temperature responses in CFRAM. In sections 3.3-3.6, we will
499 discuss the different feedbacks separately in more detail, at this point we give
500 an overview of the general effects and relative importance of the different
501 feedback processes.

502
503 It can be seen that the direct forcing of the changed CO₂-concentration alone,
504 as calculated by CFRAM, would lead to an even stronger cooling in the
505 middle atmosphere. Globally, the cooling would be approximately 9 K in both
506 July and January. The cooling is being mitigated by the combined effect of the
507 different feedbacks.



508
509 Figure 2: The mean temperature responses to the changes in CO₂ and
510 various feedback processes in July (top) and January (bottom) for the
511 experiment with double CO₂ and changed SSTs in the atmosphere between
512 200 and 0.01 hPa, for polar regions (90°S-70°S and 70°N-90°N), the tropics
513 (20°S-20°N) and the global mean, for experiment with double CO₂ and
514 changed SSTs.

515
516 Figure 2 shows that ozone feedback causes significant warming, by heating
517 the middle atmosphere globally by approximately 1.5 K in both July and
518 January, and thus counteracting the cooling effect due to the direct forcing of
519 CO₂. It has been suggested in earlier studies that the ozone response to
520 changes in the CO₂-concentration will yield a radiative feedback that will
521 mitigate the cooling, which is due to the direct forcing of CO₂ (Jonsson *et al.*,
522 2004). With CFRAM, it is possible to quantify this effect and to compare it with
523 the effects of other feedbacks in the middle atmosphere.

524
525 The temperature response due to dynamical feedbacks is small in global
526 average. This can be understood as waves generally do not generate
527 momentum and heat, but redistribute these instead (Zhu *et al.*, 2016).

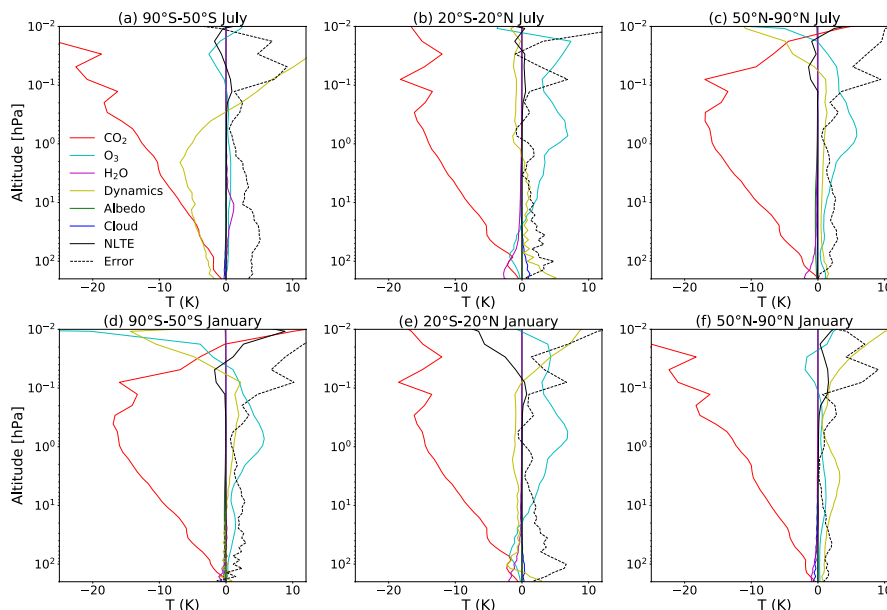


528 However, the local responses to dynamical changes in the high latitudes are
529 large, as we will see in section 3.3.
530
531 While clouds, albedo and water vapour feedbacks are of crucial importance
532 for the tropospheric and surface climate, in the middle atmosphere their role is
533 very small globally. The feedback due to water vapour shows some
534 contribution locally, as will be discussed in section 3.6. There are some small
535 temperature responses due to non-LTE effects as well.
536
537 The error term is relatively large. In CFRAM, we assumed that the radiative
538 perturbations can be linearized by neglecting the higher order terms of each
539 thermodynamic feedback and the interactions between these feedbacks, this
540 yields an error. Cai and Lu (2009) show that this error is larger in the middle
541 atmosphere than for similar calculations in the troposphere. In the middle
542 atmosphere, the density of the atmosphere is smaller, which leads to smaller
543 numerical values of the diagonal elements of the Planck feedback matrix. As
544 a result, the linear solution is very sensitive to forcing in the middle
545 atmosphere. Another part of the error is due to the fact that the radiative
546 scheme. The scheme we use in CFRAM is relatively simple, as compared to
547 the one that is used in WACCM.
548
549 Figure 2 does not only show the global mean temperature responses, but also
550 those in the polar regions and the tropics to give a more complete picture. It
551 can be seen that the total temperature response in WACCM in the winter
552 polar region (-7.7 K) is much stronger than in the summer polar region (-4.6 K)
553 during July, resulting in 3.1 K difference. In January, there is also a larger
554 temperature response in the winter polar region as compared to the summer
555 polar region, although the difference in the temperature response is only 0.6K.
556
557 It is observed that the total temperature change in the polar regions during the
558 local winter is stronger than that in local summer. At the same time, the
559 cooling due to the direct forcing of CO₂ alone is stronger in the summer polar
560 region than in the winter polar region. The strong CO₂ cooling effect in the
561 summer polar region is mitigated by the warming caused by the ozone
562 feedback.
563
564 In addition, the vertical profile of the temperature response to various
565 feedbacks is shown in Figure 3. Here, one can see that the increase in CO₂
566 leads to a cooling over almost the whole middle atmosphere: an effect that
567 increases with height. We also observe that in the summer upper mesosphere
568 regions, the increased CO₂-concentration leads to a warming. Ozone leads to
569 a warming almost everywhere in the atmosphere. In some places, this
570 warming exceeds 5 K. In the polar winter the effect of ozone is small due to
571 lack of sunlight.
572
573 There is also a relatively large temperature response to the changes in
574 dynamics. In Fig. 3, it can be seen that there is a cooling in the summer
575 mesosphere, while there is warming in the winter mesosphere. The water
576 vapour, cloud and albedo feedback play only a very small role in the middle
577 atmosphere, as we observed in Figure 2. The Non-LTE effects are also small,



578 but start to play a small role above 0.1 hPa, the exact mechanism of which is
579 outside the scope of this paper.

Temperature responses to different feedback processes



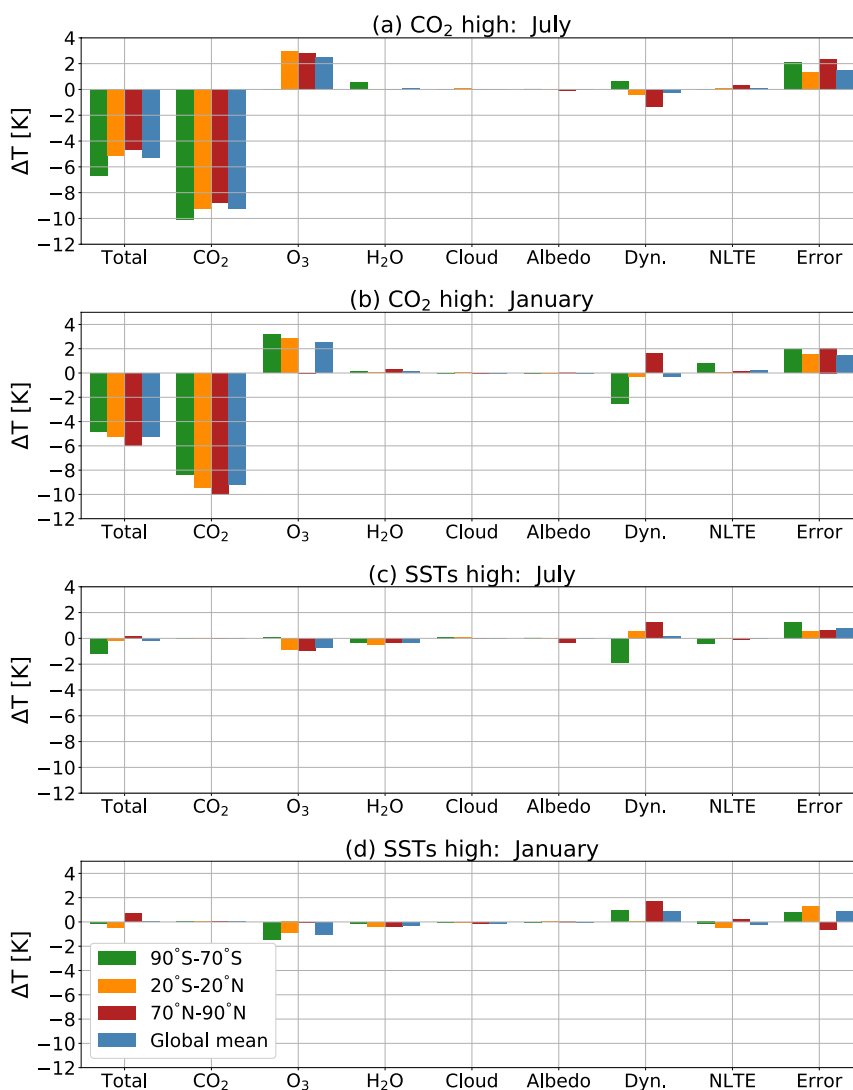
580
581 Figure 3: Vertical profiles of the temperature responses to the changes in CO₂
582 and various feedback processes in July (top) and January (bottom) for the
583 experiment with double CO₂ and changed SSTs in the atmosphere between
584 200 and 0.01 hPa, for regions from 50° N/S polewards and the tropics (20°S-
585 20°N), as calculated by CFRAM.

586
587 Figure 4 shows temperature responses for the experiment with double CO₂
588 (a,b) and changed SSTs (c,d) separately. Again, the 'total'-column shows the
589 temperature changes as found by WACCM, the columns CO₂, O₃, H₂O, cloud,
590 albedo, dynamics, Non-LTE shows the temperature responses as calculated
591 by CFRAM. Error shows the difference between temperature change in
592 WACCM and the sum of the calculated temperature responses in CFRAM.

593
594 The effects of the changed SSTs on the middle atmosphere are relatively
595 small as compared to the effects of changing the CO₂. The temperature
596 response to the water vapour feedback is, however, almost solely due to
597 changes in the SSTs.

598
599 Earlier, we discussed that the sum of the two separate temperature changes
600 in the experiment with double CO₂ and changed SSTs is approximately equal
601 to the changes observed in the combined simulation. We find that the same is
602 true for the temperature responses to the different feedback processes.

603
604 In the rest of the paper, we discuss the temperature responses to the direct
605 forcing and the various feedbacks during July and January in further detail.



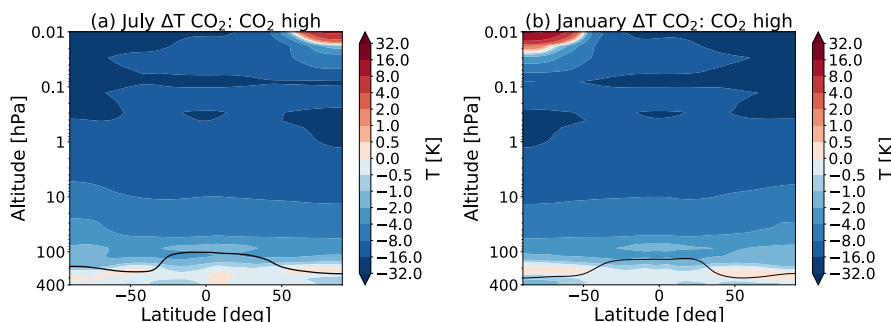
606
607 Figure 4: The mean temperature responses to the changes in CO₂ and
608 various feedback processes in July (a,c) and January (b,d) in the atmosphere
609 between 200 and 0.01 hPa, for polar regions (90°S-70°S and 70°N-90°N), the
610 tropics (20°S-20°N) and the global mean for the experiment with double CO₂
611 (a,b) and changed SSTs (c,d) separately.

612 613 3.2 Temperature direct response to CO₂

614
615 In Figure 5, we see that increasing CO₂ leads to a cooling almost everywhere
616 in the middle atmosphere, except in the cold summer upper mesosphere. The
617 higher the temperature, the more cooling there is taking place due to the
618 increasing CO₂-concentration (*Shepherd, 2008*). The reason for this is that



619 the outgoing longwave radiation strongly depends on the Planck blackbody
620 emission (Zhu *et al.*, 2016).
621



622
623 Figure 5: Temperature changes to direct CO₂ forcing in July (left) and January
624 (right) for the high CO₂ simulation as compared to pre-industrial control
625 simulation, as calculated by CFRAM. The black line indicates the tropopause
626 height for the runs with changed CO₂-concentration.
627

628 Changing the SSTs does not lead to a change in CO₂-concentration, therefore
629 the temperature response to changes in CO₂ is not present for the run with
630 only changed SST (Figures not shown). We observed that the temperature
631 responses to CO₂ and changed SST are approximately linearly additive, which
632 means that the temperature response to CO₂ in the combined experiment is
633 equal to the temperature response to CO₂ alone.
634

635 3.3 Dynamical feedback

636
637 Ozone is the largest feedback, which mitigates the cooling due to the direct
638 CO₂ forcing in most parts of the middle atmosphere (Fig. 2). Climate change
639 affects stratospheric ozone through changes in middle atmospheric chemistry,
640 through changes in dynamics or a combination of these two factors. To
641 understand how the ozone concentration is changing, it is necessary to
642 understand how the dynamics in the middle atmosphere is altered in a double
643 CO₂ climate. Therefore, we will first go into the dynamics of the middle
644 atmosphere and the temperature responses to dynamical changes.

645 The transport of air in the stratosphere and mesosphere is controlled by the
646 the Brewer-Dobson circulation (BDC). The Brewer-Dobson circulation
647 consists of rising motion in the tropics, poleward flow in the stratosphere and
648 sinking motion in the middle and high latitudes. The BDC in the mesosphere
649 spans from the summer to the winter pole (Butchart *et al.* 2010).

650 The zonal mean residual circulation forms an important component of the
651 mass transport by the BDC. It consists of a meridional (\bar{v}^*) and a vertical (\bar{w}^*)
652 component as defined in the Transformed Eulerian Mean (TEM) framework.
653 The residual circulation consists of a shallow branch which controls the
654 transport of air in the tropical lower stratosphere, as well as a deep branch in
655 the mid-latitude upper stratosphere and mesosphere.



656 Both of these branches are driven by atmospheric waves. In the winter
657 hemisphere, planetary Rossby waves propagate upwards into the
658 stratosphere, where they break and deposit their momentum on the zonal
659 mean flow, which in turns induces a meridional circulation. The two-cell
660 structure in the lower stratosphere, which is present all-year round, is driven
661 by synoptic waves. The circulation is also affected by orographic gravity wave
662 drag in the stratosphere and by non-orographic gravity wave drag in the upper
663 mesosphere (*Oberländer et al.*, 2013).

664 Most climate models show that the BDC and the upwelling in the equatorial
665 region will speed up due to an increase in CO₂-concentration (*Butchart et al.*,
666 2010). It has been shown that the strengthening of the Brewer-Dobson
667 circulation in the lower stratosphere is caused by changes in transient
668 planetary and synoptic waves, while the upper stratospheric changes are due
669 to changes in the propagation properties for gravity waves (*Oberländer et al.*,
670 2013).

671 It has been explained that the increased stratospheric resolved wave drag is
672 caused by an increase of the meridional temperature gradient in the
673 stratosphere, which leads to a strengtening of the upper flank of the
674 subtropical jets. This in turn shifts the critical layers for Rossby wave breaking
675 upward, which allows for more Rossby waves to reach the lower stratosphere,
676 where they break and deposit their momentum, enhancing the BDC
677 (*Shepherd and McLandress*, 2011)

678 The changes in the meridional component of the residual circulation (\bar{v}^*) for
679 the different simulations are shown in Fig. 6. Figure 6b and 6e show that only
680 doubling the CO₂ leads to a stronger pole-to-pole flow in the mesosphere.
681 Changing the SSTs also leads to changes in the residual circulation as can be
682 seen in Fig. 6c and 6f. *Oberländer et al.* (2013) have shown that the rising
683 CO₂-concentration affects the upper stratospheric layers, while the signals in
684 the lower stratosphere are almost completely due to changes in sea surface
685 temperature. The warmer sea surface temperatures enhance the activity of
686 transient planetary waves and orographic gravity waves in the lower and
687 middle stratosphere. The changed SSTs also leads to enhanced dissipation of
688 planetary waves, as well als orographic and non-orographic waves in the upper
689 stratosphere.

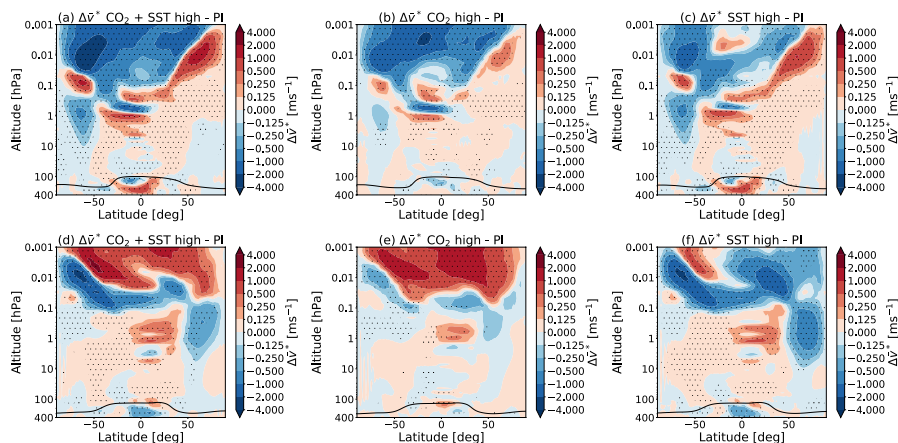
690

691

692

693

694

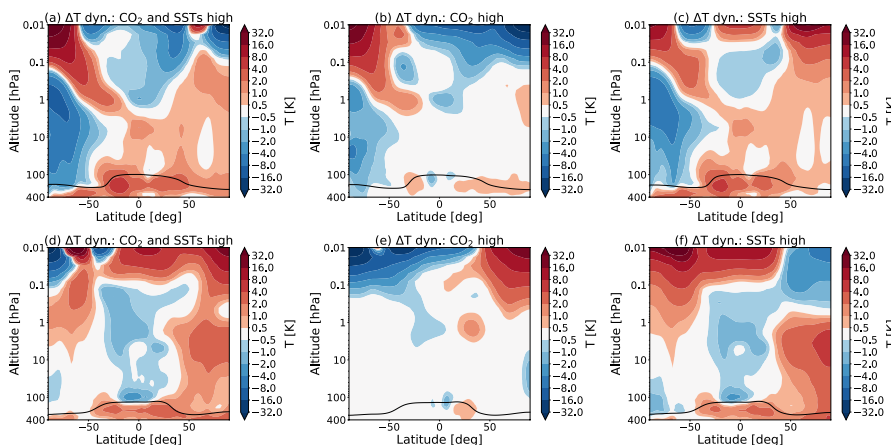


695
696 Figure 6: The changes in transformed Eulerian-mean residual circulation
697 horizontal velocity \bar{v}^* in July (top) and January (bottom) for (a,d) the
698 simulation with high CO_2 and SSTs, (b,e) the simulation with high CO_2 , (c,f)
699 the simulation with high SSTs, all as compared to pre-industrial control
700 simulation, as found by WACCM. The dotted regions indicate the regions
701 where the data reaches a confidence level of 95%. The black line indicates
702 the tropopause height for the runs with changed CO_2 -concentration and SSTs
703 (a,d), with changed CO_2 -concentration (b,e) and with changed SSTs (c,f).

704 We are interested in the temperature responses due to the dynamical
705 feedbacks in the different experiments. These temperature responses are
706 shown in Figure 7. Figure 7b and 7e show that there is cooling in the summer
707 mesosphere, while there is warming in the winter mesosphere, which is
708 consistent with a stronger summer-to-winter pole flow.

709 Figure 7c and 7f show the temperature responses due to changes in the
710 SSTs. It is seen that there is mostly a warming in the summer mesosphere
711 and mostly a cooling in the winter hemisphere, which would weaken the effect
712 of the changed CO_2 -concentration. Most of the temperature responses in the
713 lower stratosphere are caused by the changes in SSTs, as expected.

714
715
716



717

718 Figure 7: Temperature responses to changes in dynamics, as calculated by
719 CFRAM, in July (top) and January (bottom) for (a,d) the simulation with high
720 CO₂ and SSTs, (b,e) the simulation with high CO₂, (c,f) the simulation with
721 high SSTs, all as compared to pre-industrial control simulation. The black line
722 indicates the tropopause height for the runs with changed CO₂-concentration
723 and SSTs (a,d), with changed CO₂-concentration (b,e) and with changed
724 SSTs (c,f).

725 In summary, doubling the CO₂ leads to a stronger pole-to-pole flow in the
726 mesosphere, which leads to cooling of the summer mesosphere and a
727 warming of the winter mesosphere. Changing the SSTs weakens this effect,
728 but leads to temperature changes in the stratosphere and lower mesosphere.

729 3.4 Ozone feedback

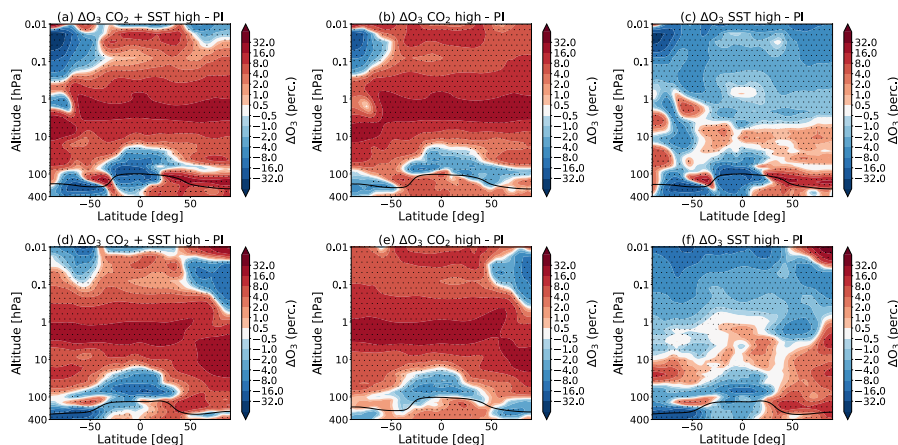
730
731 The ozone concentration in the middle atmosphere is for a large part
732 determined by so-called Chapman reactions, in which molecular oxygen (O₂)
733 is photodissociated to two atomic oxygen atoms, which may recombine in a
734 three-body process or react with molecular oxygen to produce ozone
735 (Brasseur and Solomon, 2005).

736
737 Changes in the circulation and dynamical transport have a significant impact
738 on the ozone distribution (Salby et al., 2011, Weber et al., 2011). The O₃-
739 concentration is further determined by interactions between other chemical
740 constituents, which are also impacted when the CO₂-concentration is
741 increased (Brasseur and Solomon, 2005).

742
743 Fig. 8 shows the percentage changes in O₃-concentration when the CO₂-
744 concentration and/or the SSTs change. An increase in CO₂, leads to an
745 increase of ozone in most of the middle atmosphere. However, in the tropical
746 lower stratosphere, the summer polar mesosphere, the winter and equatorial
747 mesosphere, a decrease in ozone is seen. Fig. 8c and f show that changing
748 the SSTs also has a significant impact on the ozone concentration. A



749 complete account of the ozone changes is out of the scope of this paper, but
750 the main processes responsible for ozone changes will be discussed.
751



752
753 Figure 8: The percentage changes in ozone concentration in July (top) and
754 January (bottom) for (a,d) the simulation with high CO₂ and SSTs, (b,e) the
755 simulation with high CO₂, (c,f) the simulation with high SSTs, all as compared
756 to the pre-industrial control simulation, as found by WACCM. The dotted
757 regions indicate the regions where the data reaches a confidence level of
758 95%. The black line indicates the tropopause height for the runs with changed
759 CO₂-concentration and SSTs (a,d), with changed CO₂-concentration (b,e) and
760 with changed SSTs (c,f).

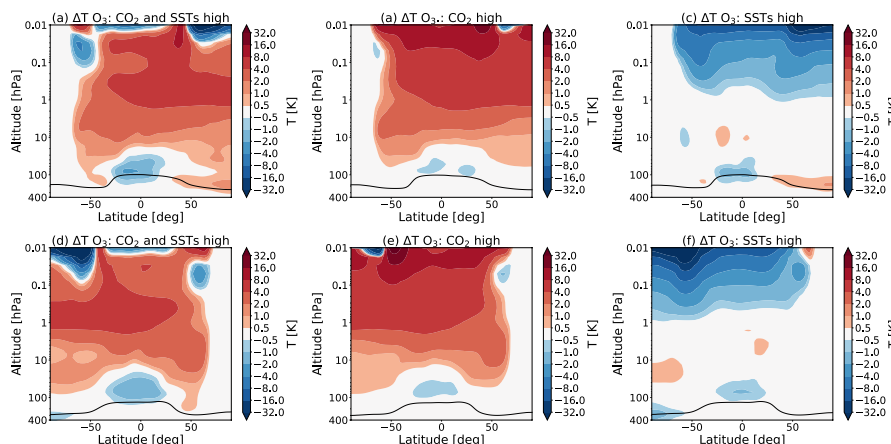
761
762 The increase in ozone due to an increase in CO₂, has been shown to be
763 primarily a result of the temperature dependence of the reaction $O + O_2 + M$
764 $\rightarrow O_3 + M$ (Jonsson *et al.*, 2004). In the upper stratosphere, ozone destruction
765 is slowed down, and leads to an increase in O₃ (Bekki *et al.*, 2011). The
766 decrease of ozone at the high latitudes in the summer mesosphere, is due to
767 a decrease in atomic oxygen which results from increased upwelling.
768 The decrease in O₃ concentration in the polar winter around 0.1 hPa is due to
769 a stronger subsidence of NO and Cl, which are both ozone-destroying
770 constituents (Schmidt *et al.*, 2006).

771
772 In addition to changes in the chemistry in the middle atmosphere, we have
773 seen that the dynamics are changing, which leads to changes in the ozone
774 concentration. The BDC affects the O₃-concentration directly, but also
775 determines the amount of ozone depleting species. The decrease in the
776 ozone concentration in the tropical lower stratosphere is due to an
777 acceleration of the BDC. In a similar fashion, the ozone concentration in
778 middle and high latitudes is increased (Braesicke *et al.*, 2018). As can be
779 seen in Fig. 8, the decrease of the O₃-concentration in the tropical upper
780 troposphere region is mainly associated with changes in the SSTs.

781
782 The temperature responses due to the ozone feedback are shown in Figure 9.
783 It can be seen that there is a warming in the regions, where there is an
784 increase of the O₃-concentration, while there is a cooling for the regions with a



785 decrease of the O₃-concentration. However, this is not the case for the winter
786 polar region, where there is no sunlight. Note that the temperature responses
787 to the changes in CO₂- and O₃- concentration behave differently in this
788 respect: the temperature responses due to the direct forcing of CO₂ follow the
789 temperature distribution quite closely, while the temperature responses due to
790 O₃ follow the ozone concentration, as also seen by *Zhu et al.*, (2016).
791



792
793 Figure 9: Temperature responses to changes in O₃-concentration, as
794 calculated by CFRAM, in July (top) and January (bottom) for (a,d) the run with
795 high CO₂ and SSTs, (b,e) the run with high CO₂, (c,f) the run with high SSTs,
796 all as compared to pre-industrial conditions. The black line indicates the
797 tropopause height for the runs with changed CO₂-concentration and SSTs
798 (a,d), with changed CO₂-concentration (b,e) and with changed SSTs (c,f).
799

800 3.5 Water vapour feedback

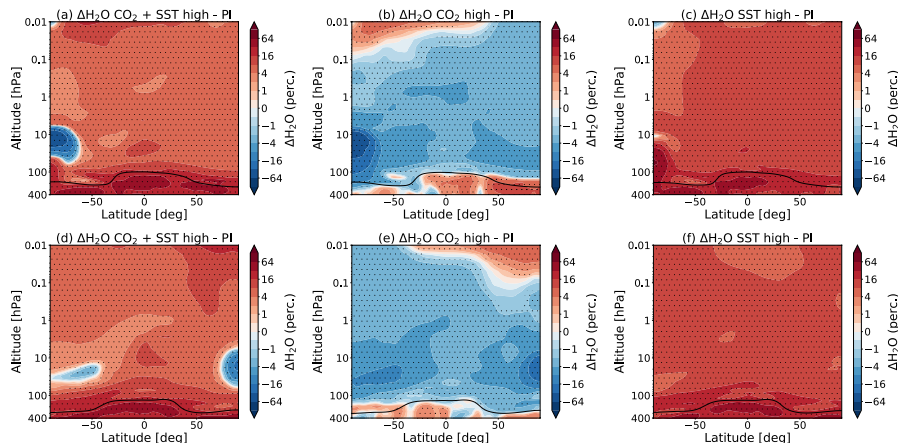
801
802 Water vapour plays a secondary but not negligible role in determining the
803 middle atmosphere climate sensitivity. In Figure 3, we saw the temperature
804 responses to the different feedbacks between 20°S and 20°N in July and
805 January for changes in both the SSTs and the CO₂-concentration. It can be
806 seen that in part of the lower stratosphere, H₂O is the main cooling agent
807 instead of CO₂. Above 30 hPa, the water vapour contribution to the energy
808 budget is negligible, as also seen by *Fomichev et al.* (2007).
809

810 Figure 10 shows how the water vapour is changing in the middle atmosphere
811 if the CO₂-concentration and/or the SSTs are enhanced. Increasing the CO₂-
812 concentration alone leads to a decrease of water vapour in most of the middle
813 atmosphere. This is due to the decrease in temperature in the tropical
814 tropopause for the double CO₂ experiment in WACCM of about -0.25 K. The
815 cold temperatures in the tropical tropopause lead to a reduction of water
816 vapour of between 2 and 8% due to freeze-drying in this region.
817

818 It can be seen that changing the SSTs leads to an increase in water vapour
819 almost everywhere in the middle atmosphere (Fig. 10c and f). The increase in
820 SSTs leads a higher and warmer tropopause, which can explain this increase

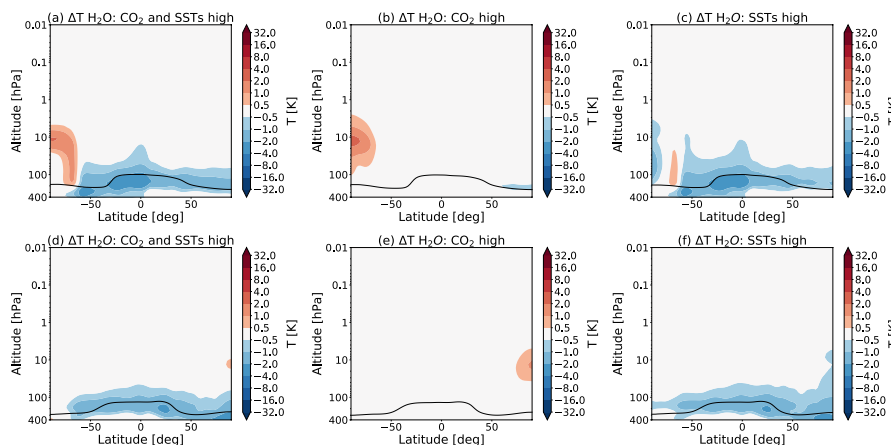


821 of water vapour. There is a considerable decrease in water vapour in the
822 winter polar stratosphere in the experiment with only doubling CO₂. The same
823 phenomenon is seen for the experiment with double CO₂ and changed SSTs.
824



825
826 Figure 10: The percentage changes in water vapour ratio in July (top)
827 and January (bottom) for (a,d) the run with high CO₂ and SSTs, (b,e) the run
828 with high CO₂, (c,f) the run with high SSTs, all as compared to pre-industrial
829 conditions, as found by WACCM. The dotted regions indicate the regions
830 where the data reaches a confidence level of 95%. The black line indicates
831 the tropopause height for the runs with changed CO₂-concentration and SSTs
832 (a,d), with changed CO₂-concentration (b,e) and with changed SSTs (c,f).
833

834 Figure 11 shows the temperature responses due to the changes in water
835 vapour. It can be seen that the regions where there is an increase (decrease)
836 in the water vapour, there is a cooling (warming). An increase (decrease) in
837 water vapour in the middle atmosphere leads to an increase (decrease) in
838 longwave emissions of water vapour in the mid and far-infrared, which leads
839 to a cooling (warming) (Brasseur and Solomon, 2005). Higher up in the
840 atmosphere, there are large percentage changes in water vapour, but the
841 absolute concentration of water is small there, which explains why there is no
842 temperature response to these changes.



843
844 Figure 11: Temperature responses to changes in H₂O-concentration in July
845 (top) and January (bottom) for (a,d) the run with high CO₂ and SSTs, (b,e) the
846 run with high CO₂, (c,f) the run with high SSTs, all as compared to pre-
847 industrial conditions, as calculated by CFRAM. The black line indicates the
848 tropopause height for the runs with changed CO₂-concentration and SSTs
849 (a,d), with changed CO₂-concentration (b,e) and with changed SSTs (c,f).

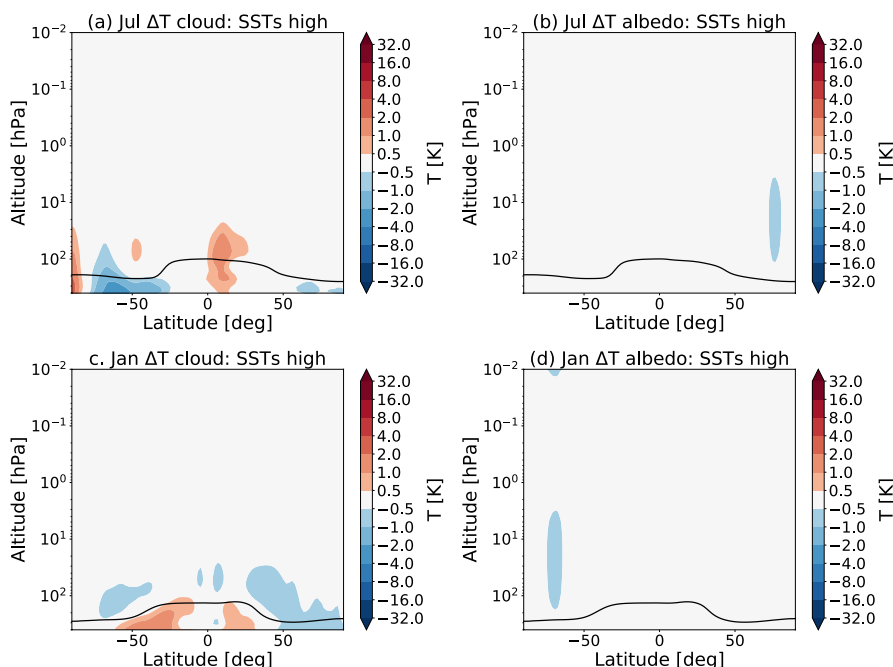
851 3.6 Cloud and albedo feedback

852
853 It is known that feedbacks due to changes in clouds and surface albedo play a
854 crucial role in determining the tropospheric and surface climate (Boucher *et*
855 *al.*, 2013, Royer *et al.*, 1990). We have seen in Figure 2 that these feedbacks
856 play only a very small role in the middle atmosphere temperature response to
857 the doubling of CO₂ and SSTs. However, there are some small radiative
858 effects from the cloud and albedo feedback, that are the result of the changes
859 in SSTs, as shown in Figure 12.

860
861 Changes in SSTs yield an overall increase in the cloud cover in the upper
862 troposphere, while this is not the case if one only increases the CO₂
863 concentration. We see that in the tropical region there is a warming due to
864 changes in clouds, while there is a cooling at higher latitudes in July (see
865 Figure 12a). In January, the pattern looks slightly different (see Figure 12c).
866 These temperature changes are due to changes in the balance between the
867 increased reflected shortwave radiation and the decrease of outgoing
868 longwave radiation.

869
870 We also see an effect of the changes in surface albedo in the stratosphere
871 (see Figure 12 b and d). The temperature responses shown in Figure 12 b
872 and d are due to radiative changes. The decrease in surface albedo would
873 cause less shortwave radiation being reflected. We suggest that this leads to
874 the cooling seen in the summer polar stratosphere, but more research is
875 needed.

876



877
878 Figure 12: Temperature responses to changes in cloud (left) and albedo
879 (right) in July (top) and January (bottom) for the run with high SSTs as
880 compared to pre-industrial conditions, as calculated by CFRAM. The black
881 line indicates the tropopause height for the runs with changed SSTs.
882

883 4. Discussion and conclusions

884
885 In this study, we have applied the climate feedback response analysis method
886 to climate sensitivity experiments performed by WACCM. We have examined
887 the middle atmosphere response to CO₂ doubling with respect to the pre-
888 industrial state. We also investigated the combined effect of doubling CO₂ and
889 subsequent warming SSTs, as well as the effects of separately changing the
890 CO₂ and the SSTs.

891
892 It was seen before that the sum of the two separate temperature changes in
893 the experiment with only changed CO₂ and only changed SSTs is, at first
894 approximation, equal to the changes observed in the combined simulation
895 (see e.g. *Fomichev et al. (2007)* and *Schmidt et al. (2006)*). This is also the
896 case for WACCM.

897
898 We have found that, even though changing the SSTs yields significant
899 temperature changes over a large part of the middle atmosphere, the effects
900 of the changed SSTs on the middle atmosphere are relatively small as
901 compared to the effects of changing the CO₂ without changes in the SSTs.
902

903 We also have seen that the cooling due to the direct forcing of CO₂ alone
904 would lead to a cooling of about 9 K between 200 and 0.01 hPa (~10–80 km),
905 for both January and July. However, the cooling in this region for the



906 experiment with a high CO₂ and SSTs is only 5.2 K in January and 5.5 K in
907 July. This means that the cooling due to the direct forcing of CO₂ is being
908 mitigated by the combined effect of the different feedback processes.

909
910 Different chemical components, in particular ozone, respond to changes in
911 CO₂ and/or SSTs due to changes in chemical reaction rate constants and
912 atmospheric density (due to changes in temperature) and due to the strength
913 of the up- and downwelling (*Schmidt et al.*, 2006). The ozone feedback
914 counteracts the cooling effect, by mitigating the cooling due to changes in
915 CO₂ by approximately 1.5 K in both July and January.

916
917 The ozone concentration increases in most parts of the middle atmosphere,
918 with the biggest change seen around 1 hPa. The ozone decreases in the
919 tropical lower stratosphere and certain parts of the mesosphere. The
920 temperature response of the ozone feedback follows the concentration of O₃.
921 The ozone feedback leads to a stronger warming for the case where only the
922 CO₂-concentration is changed, while the changes in SSTs weaken this effect
923 in the mesosphere.

924
925 We also have seen that the global mean temperature response due to
926 dynamical feedbacks is small, while the local responses to the changes in
927 dynamics are large. Doubling the CO₂ leads to a stronger summer-to-winter-
928 pole flow, which leads to cooling of the summer mesosphere and a warming
929 of the winter mesosphere. Changing the SSTs weakens this effect in the
930 mesosphere, but leads to temperature changes in the stratosphere and lower
931 mesosphere.

932
933 The role of the water vapour feedback in the middle atmosphere is generally
934 quite small. However, the water vapour feedback forms the largest
935 contribution to the temperature change in some regions of the lower
936 stratosphere, mainly as a result of changing SSTs. Changing the SSTs leads
937 to an increase of water vapour, which leads to a cooling in the lower
938 stratosphere. Changing the CO₂-concentration leads to a decrease in water
939 vapour, due to enhanced freeze-drying.

940
941 While the cloud and surface albedo feedbacks are of crucial importance for
942 the tropospheric and surface climate (*Boucher et al.*, 2013, *Royer et al.*,
943 1990), in the middle atmosphere their role is very small. There are some
944 temperature responses to these feedbacks, that are the result of the changed
945 SSTs.

946
947
948 It would also be interesting to investigate the exact mechanisms behind the
949 feedback processes in more detail. Some processes can influence the
950 different feedback processes, such as ozone depleting chemicals influencing
951 the ozone concentration and thereby the temperature response of this
952 feedback. Other studies have shown that a surface albedo change, which is
953 associated with sea ice loss, can influence the middle atmosphere dynamics,
954 which in turn influences the temperature response (*Jaiser et al.*, 2013). The
955 CFRAM cannot unravel the effects of these different processes.



956
957 There is also a need for a better understanding of how different feedbacks in
958 the middle atmosphere affect the surface climate. As discussed in the
959 introduction, the exact importance of ozone feedback is currently not clear
960 While this paper focused on the temperature changes in the middle
961 atmosphere, similar analysis can be done to quantify the effects of feedbacks
962 on the surface climate.

963
964 In conclusion, we have seen that CFRAM is an efficient method to quantify
965 climate feedbacks in the middle atmosphere, although some refinement of the
966 method is necessary to reduce the error in this region. The CFRAM allows for
967 separating and estimating the temperature responses due an external forcing
968 and various climate feedbacks, such as ozone, water vapour, cloud, albedo
969 and dynamical feedbacks. More research into the exact mechanisms of these
970 feedbacks could help us to understand the temperature response of the
971 middle atmosphere and their effects on the surface and tropospheric climate
972 better.

973 **Acknowledgement**

974 The computations and simulations were performed on resources provided by
975 the Swedish National Infrastructure for Computing (SNIC) at National
976 Supercomputer Center (NSC) in Linköping.

977
978 Hamish Struthers NSC is acknowledged for assistance concerning technical
979 aspects in making the WACCM code run on NSC supercomputer Tetralith.
980 We thank Qiang Zhang for helping to make the radiation model code
981 applicable to WACCM model data.

982 **References**

983
984
985
986
987 Akmaev, R.A., Fomichev, V.I. and Zhu, X.: Impact of middle-
988 atmospheric composition changes on greenhouse cooling in the upper
989 atmosphere, *J. Atmos. Sol. Terr. Phys.*, 68, 1879-1889, doi:10.1016/
990 j.jastp.2006.03.008, 2006.

991 Braesicke, P. and Neu, J. (Lead authors), and co-authors: Update on Global
992 Ozone: Past, Present, and Future. Chapter 3 in: *Scientific Assessment of*
993 *Ozone Depletion: 2018*, Global Ozone Research and Monitoring Project–
994 Report No. 58, 588 pp., World Meteorological Organization, Geneva,
995 Switzerland, 2018.

996 Bony, S., and co-authors: How well do we understand and evaluate climate
997 change feedback processes?, *Journal of Climate*, 19(15), 3445–3482,
998 doi:10.1175/JCLI3819.1, 2006.
999

1000 Boucher, O., Randall, D., and co-authors: Clouds and Aerosols, in: *Climate*
1001 *Change: The Physical Science Basis. Contribution of Working Group I to*
1002 *IPCC AR5*, edited by: Stocker T.F. and coauthors., Cambridge University
1003 Press, Cambridge, United Kingdom and New York, NY, USA, 2013.



- 1004 Brasseur, G. P., and Solomon, S.: *Aeronomy of the middle atmosphere,*
1005 *Chemistry and physics of the stratosphere*, Springer, New York, 2005.
- 1006 Brewer, A. W. (1949). Evidence for a world circulation provided by the
1007 measurements of helium and water vapour distribution in the
1008 stratosphere. *Quarterly Journal of the Royal Meteorological Society*, 75(326),
1009 351-363.
- 1010 Butchart, N., and co-authors: Chemistry–climate model simulations of twenty-
1011 first century stratospheric climate and circulation changes. *J. Climate*, 23(20),
1012 5349–5374, doi:10.1175/2010JCLI3404.1, 2010.
- 1013 Caldwell, P.M., Zelinka, M.D., Taylor, K.E., Marvel, K., 2016: Quantifying the
1014 sources of intermodal spread in equilibrium climate sensitivity, *J. Clim.* 29,
1015 513-524.
- 1016 Cai, M., and Lu, J.: A new framework for isolating individual feedback
1017 processes in coupled general circulation climate models. Part II: Method
1018 demonstrations and comparisons, *Climate dynamics*, 32(6), 887-900,
1019 doi:10.1007/s00382-008-0424-4, 2009.
- 1020
1021 Dietmüller, S., Ponater, M., and Sausen, R.: Interactive ozone induces a
1022 negative feedback in CO₂-driven climate change simulations. *Journal of*
1023 *Geophysical Research: Atmospheres*, 119(4), 1796-1805, 2014.
- 1024
1025 Dobson, G. M. B. (1956). Origin and distribution of the polyatomic molecules
1026 in the atmosphere. *Proceedings of the Royal Society of London. Series A.*
1027 *Mathematical and Physical Sciences*, 236(1205), 187-193.
- 1028
1029 Fomichev, V.I., Jonsson, A.I., De Grandpre, J., Beagley, S.R., McLandress,
1030 C., Semeniuk, K., Shepherd, T.G.: Response of the middle atmosphere to
1031 CO₂ doubling: Results from the Canadian Middle Atmosphere Model, *Journal*
1032 *of Climate*, 20(7), doi:10.1175/JCLI4030.1, 2007.
- 1033
1034 Hu, X., Y. Li, S. Yang, Y. Deng and Cai. M.: Process-based decomposition of
1035 the decadal climate difference between 2002-13 and 1984-95, *J. Climate*, 30,
1036 4373–4393, doi: 10.1175/JCLI-D-15-0742.1, 2017.
- 1037 Hurrell, J., et al.: The Community Earth System Model: A framework for
1038 collaborative research, *Bull. Am. Meteorol. Soc.*, doi:10.1175/BAMS-D-12-
1039 00121.1, 2013.
- 1040 Jaiser, R., K. Dethloff and D. Handorf: Stratospheric response to Arctic sea
1041 ice retreat and associated planetary wave propagation changes. *Tellus A:*
1042 *Dynamic Meteorology and Oceanography*, 65(1), 19375, doi:
1043 10.3402/tellusa.v65i0.19375, 2013.
- 1044 Jonsson, A.I., de Grandpré, J., Fomichev, V.I., McConnell, J.C., Beagley,
1045 S.C.: Doubled CO₂-induced cooling in the middle atmosphere: Photochemical



- 1046 analysis of the ozone radiative feedback, *Journal of Geophysical Research*,
1047 109, D24103, doi:10.1029/2004JD005093, 2004
- 1048 Kageyama M., and co-authors: The PMIP4 contribution to CMIP6 – Part 4:
1049 Scientific objectives and experimental design of the PMIP4-CMIP6 Last
1050 Glacial Maximum experiments and PMIP4 sensitivity experiments, *Geosci.*
1051 *Model Dev.*, 10, 4035–4055, doi:10.5194/gmd-10-4035-2017, 2017.
- 1052 Kinnison, D.E., Brasseur, G.P., Walters, S., Garcia, R.R. Marsh, D.R, Sassi,
1053 F., Harvey, V.L., Randall, C.E., Emmons, L., Lamarque, J.F., Hess, P.,
1054 Orlando, J.J., Tie, X.X., Randall, W., Pan, L.L., Gettelman, A., Granier, C.,
1055 Diehl, T., Niemeijer, Y., Simmons, A.J.: Sensitivity of chemical tracers to
1056 meteorological parameters in the MOZART-3 chemical transport model, *J.*
1057 *Geophys. Res.*, 112, D20302, doi:10.1029/2006JD007879, 2007.
- 1058 Lindzen, R.S.: Turbulence stress owing to gravity wave and tidal breakdown,
1059 *J. Geophys. Res.*, 86, 9707–9714, doi:10.1029/JC086iC10p09707, 1981.
- 1060 Ljungqvist, F.C., Zhang, Q., Brattström, G., Krusic, P.J., Seim, A., Li, Q.,
1061 Zhang, Q., and Moberg, A.: Centennial-scale temperature change in last
1062 millennium simulations and proxy-based reconstructions, *Journal of Climate*,
1063 doi: 10.1175/JCLI-D-18-0525.1, 2019.
- 1064
1065 Lu, J., and Cai, M.: A new framework for isolating individual feedback
1066 processes in coupled general circulation climate model. Part I: Formulation.
1067 *Climate dynamics*, 32 (6), 873–885, doi:10.1007/s00382-008-0425-3, 2009.
- 1068
1069 Manabe, S., & Strickler, R. F.: Thermal equilibrium of the atmosphere with a
1070 convective adjustment. *Journal of the Atmospheric Sciences*, 21(4), 361–385,
1071 1964.
- 1072 Marsh, D.R., Mills, M.J. Kinnison, D.E., Lamarque, J.F., Calvo, N., Polvani,
1073 L.M.: Climate change from 1850 to 2005 simulated in CESM1(WACCM), *J.*
1074 *Climate*, 26, 7372–7391, doi:10.1175/JCLI-D-12-00558.1, 2013.
- 1075 Marsh, D.R., Lamarque, J.-F., Conley, A.J. and Polvani, L.M., Stratospheric
1076 ozone chemistry feedbacks are not critical for the determination of climate
1077 sensitivity in CESM1(WACCM), *Geophys. Res. Lett.*, 43, 3928–3934,
1078 doi:10.1002/2016GL068344, 2016.
- 1079 McFarlane, N.A., The effect of orographically excited wave drag on the
1080 general circulation of the lower stratosphere and troposphere, *J. Atmos. Sci.*,
1081 44, 1775–1800, doi:10.1175/15200469(1987)044<1775:TEOOEG>2.0.CO;2,
1082 1987.
- 1083 Neale, R., Richter, J., Park, S., Lauritzen, P., Vavrus, S., Rasch, P. and
1084 Zhang, M: The mean climate of the Community Atmosphere Model (CAM4) in
1085 forced SST and fully coupled experiments, *J. Climate*, 26, 5150–5168,
1086 doi:10.1175/JCLI-D-12-00236.1, 2013.



- 1087 Noda, S., Kodera, K., Adachi, Y., Deushi, M., Kitoh, A., Mizuta, R., Murakami,
1088 S., Yoshida, K., Yoden, S.: Impact of interactive chemistry of stratospheric
1089 ozone on Southern Hemisphere paleoclimate simulation. *Journal of*
1090 *Geophysical Research: Atmospheres*, 122(2), 878-895,
1091 doi:10.1002/2016JD025508, 2017.
- 1092 Nowack, P.J., Abraham, N.L., Maycock, A.C., Braesicke, P., Gregory, J.M.,
1093 Joshi, M.M., Osprey, A., Pyle, J.A.: A large ozone-circulation feedback and its
1094 implications for global warming assessments, *Nature Climate Change*, 5 (1),
1095 41-45, 2015, doi:10.1038/NCLIMATE2451, 2015.
- 1096 Nowack, P.J., Abraham, N.L., Braesicke, P. and Pyle, J.A.: The impact of
1097 stratospheric ozone feedbacks on climate sensitivity estimates. *Journal of*
1098 *Geophysical Research: Atmospheres*, 123(9), 4630-4641,
1099 doi:10.1002/2017JD027943, 2018.
- 1100
1101 Oberländer, S., Langematz, U. and Meul, S.: Unraveling impact factors for
1102 future changes in the Brewer-Dobson circulation, *Journal of Geophysical*
1103 *Research: Atmospheres*, 118, 10296-10312, doi:10.1002/jgrd.50775, 2013.
- 1104 Ramaswamy, V., Collins, W., Haywood, J., Lean, J., Mahowald, N., Myhre,
1105 G., Naik, V., Shine, K.P., Soden, B., Stenchikov, G., Storelvmo, T., 2019:
1106 Radiative forcing of climate: The historical evolution of the radiative forcing
1107 concept, the forcing agents and their quantification, and application, *Meteorol.*
1108 *Monogr.* 59, 14.1 14.99. Revell, L.E., Bodeker, G.E., Huck, P. E., Williamson,
1109 B.E. and Rozanov, E.: The sensitivity of stratospheric ozone changes through
1110 the 21st century to N₂O and CH₄. *Chem. Phys.*, 12(23), 11309-11317,
1111 doi:10.5194/acp-12-11309-2012, 2012.
- 1112 Richter, J.H., Sassi, F., Garcia, R.R.: Toward a physically based gravity wave
1113 source parameterization in a general circulation model, *J. Atmos. Sci.*, 67,
1114 136-156, doi:10.1175/2009JAS3112.1, 2010.
- 1115 Rieger, V.S., Dietmüller, S., Ponater, M., 2017: Can feedback analysis be
1116 used to uncover the physical origin of climate sensitivity and efficacy
1117 differences? *Clim. Dyn.* 49, 2831-2844.
- 1118 Royer, J.F., Planton, S., Déqué, M.: A sensitivity experiment for the removal
1119 of Arctic sea ice with the French spectral general circulation model, *Climate*
1120 *Dynamics*, 5(1), 1-17, doi:10.1007/BF00195850, 1990.
- 1121
1122 Salby, M., Titova, E., Deschamps, L., Rebound of Antarctic ozone,
1123 *Geophysical Research Letters*, 39(9), doi:10.1029/2011GL047266, 2011.
- 1124
1125 Schmidt, H., Brasseur, G.P, Charron, M., Manzini, E., Giorgetta, M.A., Diehl,
1126 T., Fomichev, V., Kinnison, D., Marsh, D., Walters, S., The HAMMONIA
1127 Chemistry Climate Model: Sensitivity of the mesopause region to the 11-year
1128 solar cycle and CO₂ doubling, *Journal of Climate* 19(16), 3903-3931,
1129 doi:10.1175/JCLI3829.1, 2006.



- 1130 Shepherd, T.G.: Dynamics, stratospheric ozone and climate change,
1131 *Atmosphere-Ocean*, 46,1, 117-138, doi:10.3137/ao.460106, 2008.
- 1132 Shepherd, T.G., and McLandress, C.: A robust mechanism for strengthening
1133 of the Brewer–Dobson circulation in response to climate change: critical layer
1134 control of subtropical wave breaking. *Journal of the Atmospheric Sciences*,
1135 68, 4, 2009, doi:10.1175/2010JAS3608, 2011.
- 1136 Sigmond, M., Siegmund, P.C., Manzini, E. and Kelder, H.: A simulation of the
1137 separate climate effects of middle-atmospheric and tropospheric CO₂
1138 doubling, *Journal of Climate*, 17(12), 2352-2367, doi:10.1175/1520-
1139 0442(2004)017<2352:ASOTSC>2.0.CO;2, 2004.
- 1140 Soden, B., Held, I.M., 2006: An assessment of climate feedbacks in coupled
1141 ocean- atmosphere models, *J. Clim.* 19, 3354-3360.
- 1142 Song, X., and Zhang, G.J.: Role of climate feedback in El Niño-like SST
1143 response to global warming, *J. Climate*, 27, 7301–7318,
1144 doi:10.1175/JCLI-D-14-00072.1, 2014
1145
- 1146 Taylor, K.E., Stouffer R.J., and Meehl, G.: An overview of CMIP5 and the
1147 experimental design, *Bull. AM. Meteorol. Soc*, 93, 485-498, doi:
1148 10.1175/BAMS-D-11-00094.1, 2012.
1149
- 1150 Taylor, P.C., Cai, M., Hu, A., Meehl, J., Washington, W. and Zhang, G.J.: A
1151 decomposition of feedback contributions to polar warming amplification, *J.*
1152 *Climate*, 26, 7023–7043, doi:10.1175/JCLI-D-12-00696.1, 2013.
1153
- 1154 Weber, M., Dikty, S., Burrows, J.P., Garny, H., Dameris, M., Kubin, A.,
1155 Abalichin, J., and Langematz, U.: The Brewer-Dobson circulation and total
1156 ozone from seasonal to decadal time scales, *Atmos. Chem. Phys.*, 11, 11221-
1157 11235, doi:10.5194/acp-11-11221-2011, 2011.
1158
- 1159 Zhang, P., Wu, Y., Simpson, I.R., Smith, K.L., Zhang, X., De, B., and
1160 Callaghan, P.: A stratospheric pathway linking a colder Siberia to Barents-
1161 Kara Sea sea ice loss, *Science advances*, 4(7), eaat6025, doi:
1162 10.1126/sciadv.aat6025, 2018.
1163
- 1164 Zheng, J., Zhang, Q., Li, Q., Zhang, Q. and Cai, M., Contribution of sea ice
1165 albedo and insulation effects to Arctic amplification in the EC-Earth Pliocene
1166 simulation, *Clim. Past*, 15, 291-305, doi:10.5194/cp-15-291-2019, 2019.
1167
- 1168 Zhu, X., Yee, J.-H., Cai, M., Swartz, W.H., Coy, L., Aquila, V., Garcia, R.,
1169 Talaat, E.R.: Diagnosis of middle-atmosphere climate sensitivity by the
1170 climate feedback-response analysis method, *Journal of Atmospheric*
1171 *Sciences*, 73(1), 3-23, doi:10.1175/JAS-D-15-0013.1, 2016.